JOURNAL OF PROPULSION AND POWER
Vol. 24, No. 6, November–December 2008

Investigation of Supersonic Combustion with Angled Injection in a Cavity-Based Combustor

Eunju Jeong*
Seoul National University, Seoul 151-744, Republic of Korea
Sean O'Byrne†
University of New South Wales, Australian Defence Force Academy, Canberra, ACT 2600, Australia
In-Seuck Jeung‡
Seoul National University, Seoul 151-744, Republic of Korea
and
A. F. P. Houwing§
Australian National University, Canberra, ACT 0200, Australia

DOI: 10.2514/1.36519

Self-ignited supersonic combustion experiments have been performed using a cavity-based injector in the T3 free-piston shock tunnel, using various combustor inlet and fuel-flow conditions. Planar laser-induced fluorescence on the hydroxyl radical and fast-acting pressure transducers are used to investigate the flow characteristics. Four hydrogen injectors are located upstream of an open cavity. The separated shear layer reattaches, generating an oblique shock at the cavity's trailing edge and establishing the major flow structure. The normalized pressure rise due to combustion increases as the equivalence ratio increases and the freestream stagnation enthalpy decreases, over the range of conditions tested. Angled injection upstream of the cavity allows the cavity to act as a flame holder. High injection pressure helps to ignite immediately upstream of the injector and forms two flame layers over the cavity. The fluorescence peak signal shows periodic maxima near the cavity, and the interval between peaks decreases as the equivalence ratio is increased. Low-total-enthalpy conditions also exhibit longer ignition-delay distances. Comparison of fluorescence images and static pressure measurements indicates that, at these conditions, the heat release is mostly initiated by the shock wave from the cavity's trailing face and the ignition above the cavity does not have a strong influence on the downstream combustion.

Nomenclature

D	=	depth of the cavity
h_0	=	total enthalpy of nozzle reservoir
L	=	length of the cavity
M	=	Mach number
P	=	pressure
T	=	temperature
u	=	velocity
u_{shock}	=	primary shock speed
ρ	=	density
Φ	=	equivalence ratio

Subscripts

o	=	stagnation condition
∞	=	freestream condition

Presented as Paper 7918 at the 14th AIAA/AHI Space Planes and Hypersonic Systems and Technologies Conference, Canberra, Australia, 6–9 November 2006; received 8 January 2008; accepted for publication 23 May 2008.

*Graduate Student, Department of Aerospace Engineering; newaero1@snu.ac.kr. Student Member AIAA.
†Lecturer, School of Aerospace and Mechanical Engineering; s.obyrne@adfa.edu.au. Senior Member AIAA.
‡Professor, Department of Aerospace Engineering, Institute of Advanced Aerospace Technology; enjis@snu.ac.kr. Associate Fellow AIAA.
§Associate Professor, Department of Physics, Faculty of Science; frank.houwing@anu.edu.au. Member AIAA.

I. Introduction

THE scramjet is an engine being actively researched for use in aircraft and future space transportation systems operating at speeds of about Mach 4 and above. At these flight velocities, the incoming air should maintain supersonic speed within the combustor to prevent excessive dissociation of nitrogen and oxygen gases at the high temperatures caused by slowing the freestream flow to subsonic speeds. Therefore, the available time for fuel–air mixing and combustion is limited to times on the order of 1 ms, which makes maintaining supersonic combustion a difficult task [1,2]. Consequently, the realization of this engine is strongly linked to the design of fuel injection, fuel–air mixing, and combustion processes in the combustor. To this end, researchers have conducted studies into fuel injection, fuel–air mixing, and supersonic combustion over several decades, but no general consensus exists on the most efficient method of injecting fuel into a supersonic flow to ensure efficient combustion.

Several methods have been used in scramjet research for enhanced mixing and flame holding, including transverse injection from the wall, shock-enhanced mixing by generation of baroclinic torque, generation of axial vorticity of the airstream using swept-ramp injectors, and generation of streamwise vorticity using alternating wedges [3–10]. The simplest injection method is transverse injection from the wall. This method leads the fuel jet to interrupt the supersonic crossflow and results in a bow shock in front of the injector. The wall boundary layer upstream of the injector is separated, and fuel and air mix subsonically in this region [11,12]. This subsonic region plays an important role as a flame holder in transverse fuel injection. The fuel-injection method provides not only sufficient fuel–air mixing but also low aerodynamic drag in the combustor. Transverse injection, especially at high flight Mach numbers, has the disadvantage of causing large total pressure losses due to the bow shock generated by the fuel jet. A modification of the

transverse-injection scheme, dual-injection systems have a higher mixing rate and greater penetration into the airstream but have more losses of total pressure than a single-injection system [13,14]. Another method for mixing and flame holding uses a backward-facing step near the injectors [15,16]. Use of a backward-facing step helps to ignite the fuel–air mixture and generates a large subsonic recirculation region with hot gases near the fuel–air interface. This configuration can sustain combustion once it has ignited but may also cause total pressure losses in the same manner as transverse injection and increase pressure drag by the low pressure at the backward-facing step. On the other hand, angled fuel injection helps to enhance the fuel–air mixing and reduces the total pressure losses compared with normal injection by generating a weaker bow shock. The angled jet's axial momentum can also contribute to the net engine thrust [17]. Angled injection may experience significant variations in self-ignition position and flame stabilization, depending on the total enthalpy of the incoming airflow [12,18]. Lobed strut injectors have been employed with some success to improve mixing by generation of streamwise vortices in the core region of the combustion chamber [19]. In recent years, cavity fuel injection has been employed within supersonic combustors. For example, CIAM (Central Institution of Aviation Motors, Moscow) used a cavity downstream of a ramp injector and found significant improvement of the hydrocarbon combustion efficiency [20–24]. Also, several experimental studies have been published by the U.S. Air Force Research Laboratory verifying the potential of cavity injection for encouraging mixing and flame holding at flight Mach numbers around Mach 6 [25–27]. Another experimental program, conducted in the same facility as the experiments described in this paper, performed experiments in a model scramjet cavity combustor with hydrogen fuel injection from the downstream wall of the cavity in the reverse direction to about the Mach 4 incoming flow [28,29]. In that study, fluorescence of the hydroxyl (OH) radical was used to visualize the flow, and OH was shown to originate in the shear layer above the cavity. This experiment showed that there was no significant OH signal in the cavity, and injecting fuel into the cavity in a direction opposite to the airflow did not act as a flame holder. However, at the conditions investigated, hydrogen ignited very rapidly within the shear layer and flame holding was not necessary.

The main purpose of this study is to investigate the combustion characteristics of a scramjet engine using angled hydrogen injection upstream of the cavity. Hydroxyl fluorescence images and floor static pressure measurements provide information about the ignition location and the effect of heat release within the combustor caused by this injection configuration.

II. Experimental Arrangement

A. Description of the Model Cavity Supersonic Combustor

The model cavity supersonic combustor used in this study consists of a 500-mm-long rectangular duct with a constant cross section of 52 by 25 mm, as shown in Fig. 1. This model does not have any compression by intake and thrust surface, and the nozzle-exit conditions generated by the shock tunnel are designed to simulate realistic combustor entrance conditions for flight at Mach 11.4 at an altitude of 29 km. The inlet of the model scramjet combustor is located at the exit of the facility's Mach 4 contoured nozzle during the test time. The cavity is installed on the bottom wall inside the combustor, 152.5 mm downstream of the inlet. It is 5 mm deep and has a 22.5 deg rear ramp angle. The length-to-depth ratio of this cavity is 4.8, which qualifies it as an open cavity [20]. The length is defined as the distance from the cavity's leading edge to the midpoint of the rear ramp wall.

A Ludwieg tube is used for the fuel-injection system, as it provides uniform hydrogen injection conditions throughout the duration of the tunnel operation. The Ludwieg tube was filled with gaseous hydrogen fuel at room temperature and an initial fuel pressure that decides the global equivalence ratio for the experiment. A fast-acting valve was triggered from the recoil of the tunnel, opened 50 ms before the arrival of test flow in the combustor with an injection duration of 100 ms. For the freestream conditions used in these tests, the shortest steady-flow test time is 0.5 ms. The fuel-injection duration is, therefore, much greater than the test gas duration in the shock tunnel, and so the mass flow rate of fuel in the combustor is roughly constant throughout the tunnel run. The fuel is injected sonically from four 2-mm-diam ports located 20 mm upstream of the cavity's front step, at an angle of 15 deg to the horizontal. The space between injectors is 10 mm and the space between the outermost injectors and side walls is 11 mm. The total temperature of the fuel jet is ambient room temperature. UV fused silica windows were installed on the top wall and one side wall of the combustor for acquiring planar laser-induced fluorescence (PLIF) images [28]. The laser sheet enters the top window and an intensified charge-coupled device camera (Princeton Instruments PI-ICCD) captures the transmitted OH fluorescence signal through the side window.

Sixteen fast-acting piezoelectric pressure transducers (Piezotronic PCB type 113M125) were used to measure the floor static pressure during the experiment. One pressure transducer for measuring incoming flow to the combustor was located 70 mm downstream of the inlet, another pressure transducer was located within the cavity, 15 mm downstream of the cavity's leading edge, and 14 combustor-wall pressure transducers were installed from 233 mm downstream of the inlet along the centerline at intervals of 20 mm. The first six transducer locations can be seen in Fig. 1.

B. The T3 Free-Piston Shock Tunnel Facility and Flow Conditions

The experiments were performed in the Australian National University's T3 free-piston shock tunnel [30], shown schematically in Fig. 2. A free piston, driven by high-pressure air in the reservoir tube, compresses the driver gas in the compression tube, which is filled with a mixture of 20% argon and 80% helium. As the piston approaches the end of the compression tube a steel diaphragm, initially separating the test gas in the shock tube from driver gas, is ruptured by high-pressure driver gas. As soon as the steel diaphragm is ruptured, a strong shock wave propagates along the shock tube and accelerates the test gas until the gas is stopped by the shock reflection from the end of the shock tube. The high-pressure, high-temperature gas at the end of the shock tube acts as a reservoir for the Mach 4 contoured nozzle.

The shock tunnel is a pulsed facility, and test time is restricted by the shock-tube volume and the mass flow rate through the nozzle. Constant-pressure test time in T3 is typically between 0.5 and 2 ms, depending on the desired freestream total enthalpy. Two major effects that reduce the test time are initiation of uniform flow at the nozzle exit and the contamination of the test gas by the arrival of the

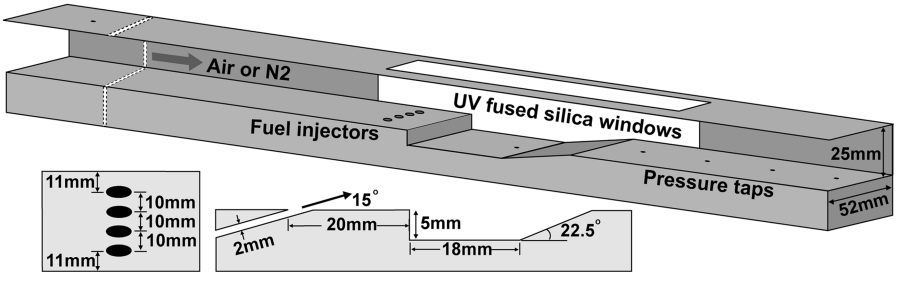

Fig. 1 Schematic of cavity scramjet combustor.

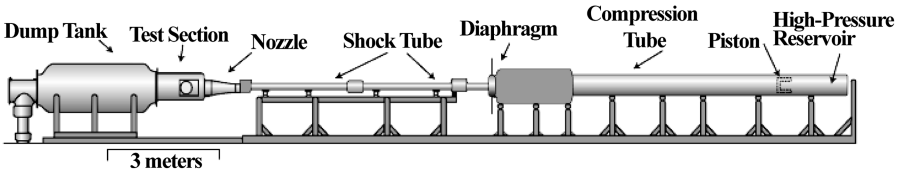

Fig. 2 T3 free-piston shock tunnel.

driver gas in the nozzle flow. According to previous T3 scramjet work [31], the test gas did not show driver gas contamination at a total enthalpy of 4 MJ/kg until more than 4 ms after shock reflection. The total enthalpy conditions for this experiment are between 3.82 and 6.45 MJ/kg, as previously mentioned, and so the incoming flow into the combustor should not be affected by the driver gas at the nominal test time of 1.5 ms. In this study, total test time was assumed to occur for 0.5 ms between 1.25 and 1.75 ms after the reflection of the shock wave at the nozzle reservoir, as the nozzle-reservoir pressure was within 2.5% of the average value throughout this interval. The laser for the PLIF imaging was triggered 1.5 ms after shock reflection, in the middle of this time interval, to allow the combustor flow sufficient time to establish. More detailed information about the T3 facility and the techniques used to determine the inflow conditions is contained in [29].

A converging–diverging nozzle is connected to the end of the shock tube to generate the Mach 4 flow. Shock speed and nozzle-reservoir pressure were measured using piezoelectric pressure transducers. These pressures are used as the inputs to the equilibrium shock-tube code (ESTC) [32] and the STUBE [33] nozzle code, to determine the flow conditions at the nozzle exit. To investigate the supersonic combustion process with different inflow conditions, the nominal fill pressure of the test gas in the shock tube determined the flow conditions at the combustor entrance. Hence, in this paper, total enthalpies of 6.45, 5.16, 4.48 and 3.82 MJ/kg were generated using different shock-tube fill pressures. The calculated stagnation and inflow conditions are summarized in Tables 1 and 2.

As mentioned in the preceding section, the equivalence ratio was changed by using different initial pressures to fill the Ludwieg tube with hydrogen gas. For example, when the total enthalpy is 6.45 MJ/kg, nominal hydrogen fuel fill pressures of 900, 1500, and 2500 kPa correspond to global fuel–air equivalence ratios of 0.13, 0.22 and 0.44, , respectively. As the total enthalpy decreases, the equivalence ratio also decreases because the air-mass flow rate increases. The detailed global equivalence ratios at each incoming flow condition are summarized in Table 3.

C. PLIF System

The hydroxyl (OH) radical is formed as an intermediate during high-temperature combustion reactions and is used as a marker of zones where the combustion is ongoing [34]. The fluorescence from OH can be used to determine where ignition occurs, an important characteristic in the design of a supersonic combustor. In OH PLIF, a frequency-doubled Nd:YAG laser operating at 532 nm is used to pump a Spectraphysics PDL2 dye laser using a mixture of rhodamine 590 and rhodamine 610 dyes that can operate over a range of wavelengths between 560 and 570 nm. The radiation from this dye laser is frequency-doubled to generate radiation between 280 and 285 nm, where $A^2\Sigma_g^+ \leftarrow X^2\Pi$ (1,0) rovibronic transitions can be excited. This laser system has a pulse duration of 8 ns. The beam is formed into a sheet using a combination of a cylindrical lens and spherical lens and passes through an aperture to generate a well-defined intensity distribution, then enters the duct. The thickness of the laser sheet is 0.32 ± 0.04 mm. This laser sheet is located above the second injector from the side window and starts from 5 mm upstream of the injector. There was no attempt to obtain quantitative OH mole fraction measurements in this study, though several corrections to the raw signal were made to make the OH signal as good a qualitative indicator of OH concentration as possible. O'Byrne et al.[28] detail the equipment used to generate and detect the PLIF signal and the image corrections used to normalize the

Table 1 Shock-tube and nozzle-reservoir flow properties

Shock-tube fill pressure, kPa	u_{shock}, km/s	h_0, MJ/kg	P_0, MPa	T_0, K
50	2.57 ± 0.03	6.45 ± 0.14	15.7 ± 0.68	4422 ± 64
75	2.36 ± 0.03	5.16 ± 0.03	15.0 ± 0.46	3855 ± 18
100	2.23 ± 0.04	4.48 ± 0.06	15.5 ± 0.28	3483 ± 37
125	2.04 ± 0.01	3.82 ± 0.06	15.4 ± 0.64	3087 ± 41

Table 2 Combustor inlet conditions

h_0, MJ/kg	P_∞, kPa	T_∞, K	ρ_∞, kg/m^3	u_∞, m/s	M_∞
6.45	111 ± 7	1667 ± 55	0.23 ± 0.01	2952 ± 28	3.71 ± 0.03
5.16	100 ± 4	1280 ± 14	0.27 ± 0.01	2680 ± 07	3.83 ± 0.01
4.48	98 ± 2	1095 ± 23	0.31 ± 0.01	2513 ± 15	3.87 ± 0.01
3.82	92 ± 4	899 ± 16	0.35 ± 0.01	2347 ± 17	3.97 ± 0.01

Table 3 Fuel-injection conditions

Fuel fill pressure, kPa	Fuel plenum pressure, kPa	Fuel-injection pressure, kPa	Equivalence ratio			
			$h_0 = 6.45$ MJ/kg	$h_0 = 5.16$ MJ/kg	$h_0 = 4.48$ MJ/kg	$h_0 = 3.82$ MJ/kg
900	631 ± 21	333 ± 11	0.13	0.13	0.12	0.11
1500	1104 ± 17	583 ± 9	0.22	–	–	–
2500	1906 ± 33	1005 ± 18	0.44	0.42	0.41	0.37

images for spatial nonuniformity in the laser sheet. The OH-PLIF signal is detected using an intensified charge-coupled device (ICCD) camera. The intensifier gate time was set to 50 ns to filter out luminosity from the tunnel flow and chemiluminescence from the combustion in the duct. A Schott WG305 filter was used in front of the camera lens to reduce the detected laser scatter and resonant fluorescence, and a UG11 filter was used to reduce the effect of broadband flow luminosity.

III. Results

A. Visualization

1. *No Fuel Injection*

The characteristics of only airflow over the cavity with no fuel injection were investigated initially, to compare with the fuel-injection case. Figure 3 is the luminosity picture, obtained in the absence of laser excitation, using nitrogen as the test gas. As shown in the left picture, the shear layer over the cavity no longer remains parallel with the floor, but deflects downward toward the rear wall of the cavity. As previous studies have shown, the boundary layer separates from the cavity's leading edge and forms a free shear layer. Here, a part of the inflow moves into the cavity and generates a recirculation zone, whereas the other part of the inflow passes over the trailing edge. Figure 3 does not indicate the presence of compression waves at the leading edge. This result is consistent with schlieren images produced by Ben-Yakar and Hanson [35]. Their research showed that the leading-edge compression waves observed for the rectangular cavities with $L/D = 3$ and 5 do not exist with an angled back wall cavity at a main-flow Mach number of 3.5 because angling the trailing face prevents strong acoustic waves from propagating longitudinally along the cavity. Therefore, in this experiment an expansion wave is generated at the leading edge, based upon the direction of the shear layer deflection. The deflected shear layer near the trailing edge reattaches at the inclined wall and creates a high-pressure region, shown by the strong luminosity signal in the image. This is consistent with the expected behavior of an open cavity. The shock wave generated at the ramp impinges on and reflects from the top wall of the duct, continuing to propagate along the duct.

2. *Nonreacting Flow*

Injecting the hydrogen fuel into a nitrogen tunnel flow allows us to investigate the effect of fuel injection and mixing in the absence of combustion. Figure 4 shows the luminosity image with fuel injection. The flow condition shown in this image has a freestream total enthalpy of $h_0 = 6.45$ MJ/kg and a fuel–air equivalence ratio of $\Phi = 0.13$. According to previous research, with mass injection in the cavity, the shear layer thickness (and momentum thickness) is sufficiently large to prevent any vortex roll up or any large downward deflections of the shear layer, thereby preventing external flow impingement upstream of the cavity's trailing face [36]. This study also supports those previous findings, and the luminosity image of Fig. 4 shows the generation of a strong oblique shock at the end of the cavity's trailing face. This results from the existence of low velocity of fuel in the cavity, and, therefore, the shear layer from the leading edge does not deflect to the middle of the cavity's trailing face, but reattaches near the end of the cavity's trailing edge, generating an oblique shock. The high-pressure and high-temperature region behind this oblique shock can also act as an ignition source.

3. *Reacting Flow*

To generate supersonic combustion in the combustor, air is used as the test gas, at the same nominal flow conditions as for the nitrogen tests described previously. This experiment has no additional ignition spark source to generate the flame and induces autoignition by the combustor inflow temperature of more than 1000 K. The supersonic flame structures vary from one tunnel run to the next, as expected for turbulent combustion, but the overall behavior is similar for different tunnel runs at the same experimental condition.

Figure 5 shows the OH-PLIF images for all equivalence ratios and total enthalpies. The vertical and horizontal plots in Fig. 5 are horizontal and vertical signal counts averaged along the height and width, respectively, of the PLIF image. These plots clearly show the extent of the combusting portion of the shear layer and the distance over which OH generation occurs in the flow. The laser sheet for OH PLIF starts from the point of fuel injection and is approximately 60 mm long. The OH signals are easily distinguishable from background luminosity and chemiluminescence. A region slightly downstream of the laser sheet is included in the images to allow a direct comparison of the relative size of the fluorescence and chemiluminescence signals. Note that for each of the images the color map has been scaled to the maximum number of camera counts for that image. This maximum value is shown next to the color bar at the top right of each image. In Fig. 5c, higher signals than the maximum count of Fig. 5b are cut off to remove some artificially high signal values at the edge of the laser sheet caused by the intensity normalization procedure and to allow for a more direct comparison between Figs. 5b and 5c. The actual maximum count of Fig. 5c is 6876. Some of the images show increased signal near the edges of the laser sheet; this is particularly apparent in Figs. 5e and 5f, where the PLIF signal is very low. This increase in signal is an artifact generated by the normalization of the OH fluorescence signal to the laser-sheet profile intensity, and low signals cause the signal-to-noise

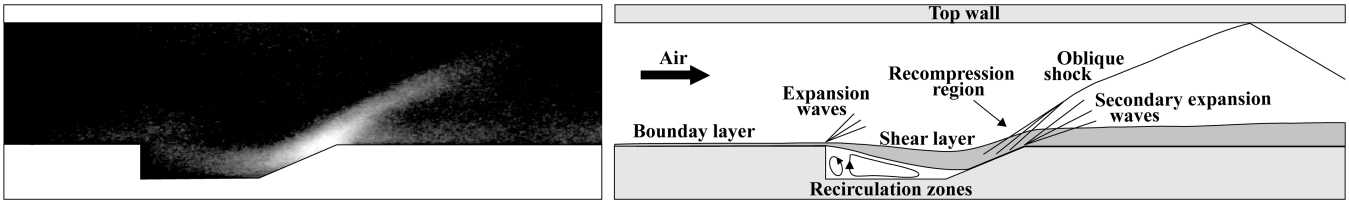

Fig. 3 Without fuel injection: a) luminosity image, b) schematic view.

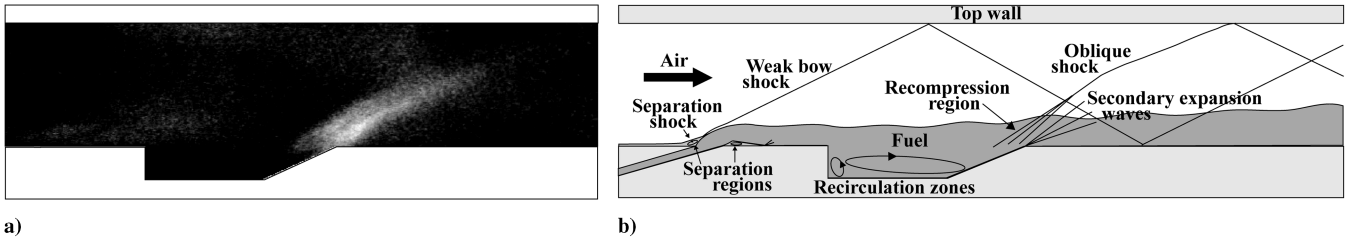

Fig. 4 Fuel injection: a) luminosity image and b) schematic view.

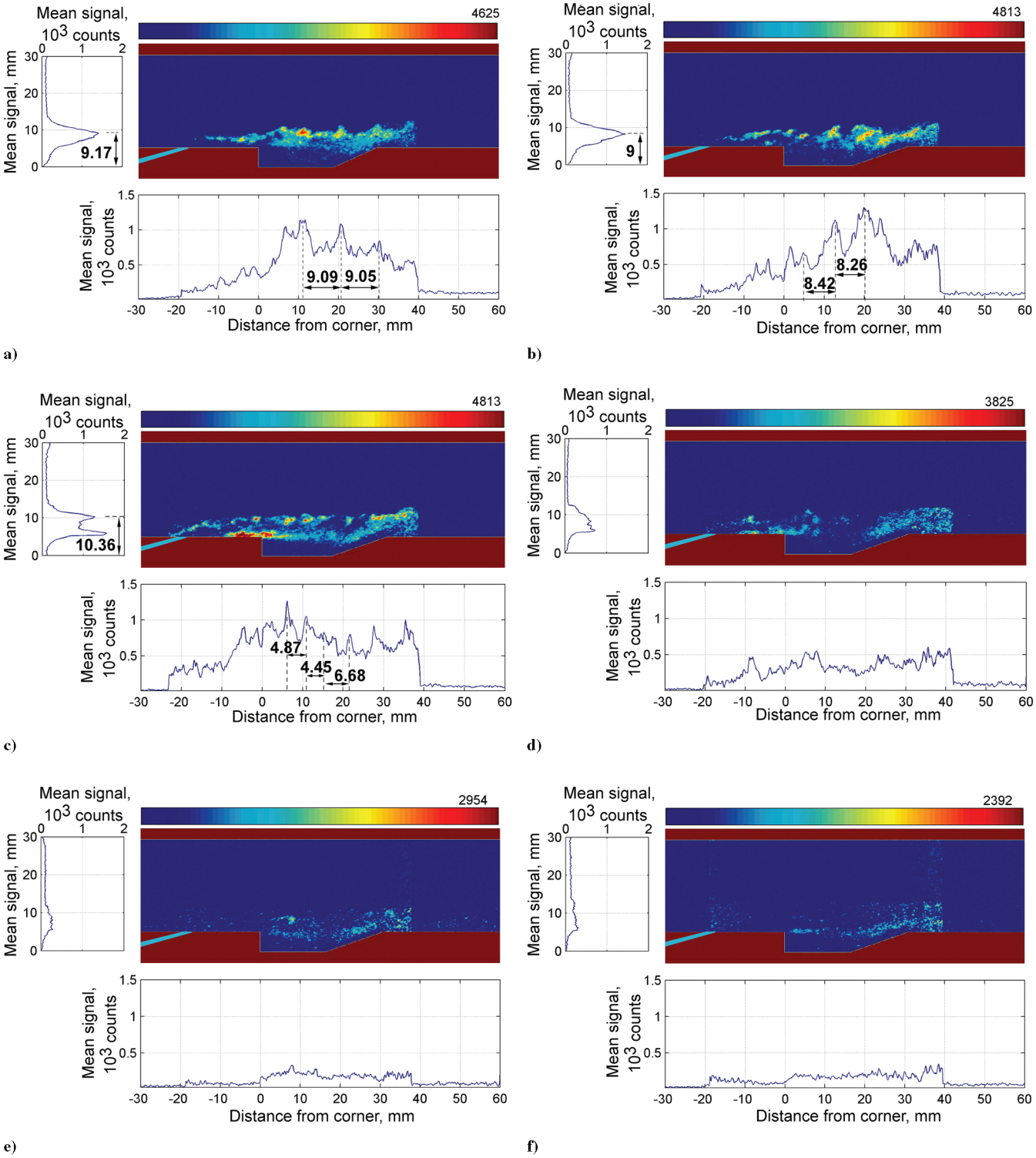

Fig. 5 OH-PLIF image near the cavity, and OH-signal distribution along the length: a) $h_0 = 6.45$ MJ/kg and $\Phi = 0.13$, b) $h_0 = 6.45$ MJ/kg and $\Phi = 0.22$, c) $h_0 = 6.45$ MJ/kg and $\Phi = 0.44$, d) $h_o = 5.16$ MJ/kg and $\Phi = 0.42$, e) $h_0 = 4.48$ MJ/kg and $\Phi = 0.41$, and f) $h_0 = 3.82$ MJ/kg and $\Phi = 0.37$.

ratio of the normalized image to be reduced. In Fig. 5a, there are very low OH fluorescence signals from the fuel injector to about 7.5 mm downstream of injection.

Generally, when fuel is injected perpendicular to the floor, a bow shock develops in front of the injector and the shock-heated air ignites the fuel [31]. In this study, the fuel is injected at an angle of 15 deg to the floor surface and does not induce as strong of a bow shock as for normal injection. At $\Phi = 0.13$, which corresponds to the lowest injection pressure used, the fuel does not achieve a high enough temperature for ignition, does not penetrate as far into the airstream as it does at the higher equivalence ratio conditions, and no OH is visible at the fuel-injector location. Even though the static temperature of the incoming air is over 1500 K, the bottom wall of the duct near the fuel injector remains near room temperature because of the room-temperature wall initial condition and short duration of the tunnel run, combined with the much lower temperature of the fuel jet. For sonic injection at a total temperature of 296 K, the fuel has a static temperature of 246 K, and so the static temperature of the mixture at the injection location is low and the flow will have a longer autoignition delay time.

At 7.5 mm downstream of the injector, the OH fluorescence signal appears, indicating that ignition occurs due to the elevated temperature of the air and shock-heated fuel in the shear layer. At $\Phi = 0.22$, shown in Fig. 5b, the OH fluorescence is apparent from 1.5 mm behind the injector, and the overall OH fluorescence signals are strong not only in the mixing layer in the middle of the duct but also in the shear layer immediately above the cavity. The incoming airflow under the fuel jet mixes with fuel in the shear layer and ignites above the cavity. Despite the relatively shallow 15 deg angle used for fuel injection, it is possible to inject the 3-dimensional jet flow into the supersonic flow field once the fuel penetrates into the airflow with the higher injection pressures. The $\Phi = 0.44$ condition, shown in Fig. 5c, illustrates this phenomenon more clearly.

High fuel-injection pressure generates a weak bow shock in front of the injector and produces the high-pressure and high-temperature conditions required to ignite the fuel behind this shock. The region immediately upstream of the injector contains OH because the recirculation zone, generated about 4 mm upstream of the injector, helps air and hydrogen fuel mix with each other at a high enough temperature to hold the flame. A region containing significant mixing due to high shear and temperature caused by the near-normal bow shock can operate as a flame holder immediately upstream of the fuel jet. High fuel-injection pressure allows the jet to penetrate further into the supersonic airflow and allows air to pass under the fuel jet, mixing more effectively. Hence, higher OH fluorescence signals appear in this region as a result of combustion, and there are two major flame layers in the vertical section image. This behavior is significantly different to the cases for $\Phi = 0.13$ (Fig. 5a) and $\Phi = 0.22$ (Fig. 5b). In Figs. 5a–5c, the peak OH interval of the repeated peak OH signal becomes shorter, that is, conditions of $\Phi = 0.13$, 0.22, and 0.44 have about 9, 8, and 4.5 mm between regions of peak OH signal, respectively. As the equivalence ratio is increased, the structures also become smaller. This intermittent occurrence of high OH signal was also noted in [28], and is caused by the excitation of acoustic modes within the cavity.

One significant difference between the images in Fig. 5 and the previous work in [28], where horizontal injection from the downstream wall was used, is a measurable amount of OH fluorescence generated within the cavity itself. This is apparent from the horizontal average plots on the vertical axes in Fig. 5. The combustor wall had close to zero average fluorescence counts, whereas the plots in Figs. 5a–5d all showed extra signals within the cavity region. This evidence supports the idea that, at least for the case of upstream injection, the cavity may be acting as a reservoir for OH radicals in this injector configuration. For the case of Fig. 5d, the OH signal is weaker compared with Figs. 5a–5c, but the boundary of the flame can still be distinguished. When compared with a similar equivalence ratio in Fig. 5c, the peak OH signal in Fig. 5d is lower, but the two-flame-layer structure and ignition near the injector are still visible. Figures 5c–5f show that as the total enthalpy is decreased, the OH signal intensities near the cavity also reduce. In fact, the OH signal can hardly be seen at all in Fig. 5f.

Given the incoming flow temperature in the combustor, it is likely that at the lower enthalpy condition the temperature of the incoming flow is not high enough to generate spontaneous ignition in the shear layer over the cavity, but combustion occurs downstream of the window, where the fuel and air are better mixed and interact with the reflected shock from the rear cavity wall. Also, overall higher fluorescence signals are shown at the cavity's trailing edge; therefore, the oblique shock from the cavity's trailing edge plays an important role in enhancing the fuel–air mixing and ignition.

B. Pressure Measurements

1. *No Fuel Injection*

Figure 6 shows the pressure distributions for the no-fuel-injection state at two different total enthalpy flow conditions (6.45 and 3.82 MJ/kg). For Figs. 6–10, the static pressure is normalized to the nozzle-reservoir pressure to remove the effect of fluctuations in the tunnel conditions during the test time. Error bars in the plots indicate the run-to-run standard deviation of the mean pressure value at each

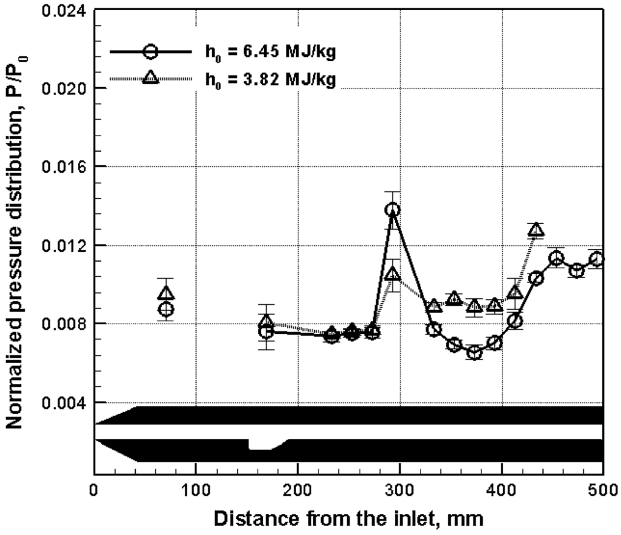

Fig. 6 Wall pressure distribution without fuel injection.

position. These fluctuations are up to 3.5 times greater than the fluctuations in an individual pressure trace over the steady-flow time in the absence of injection, indicating that the measurement errors are dominated by the facility run-to-run variations. For both total enthalpy conditions, the static pressure inside the cavity is about 12%

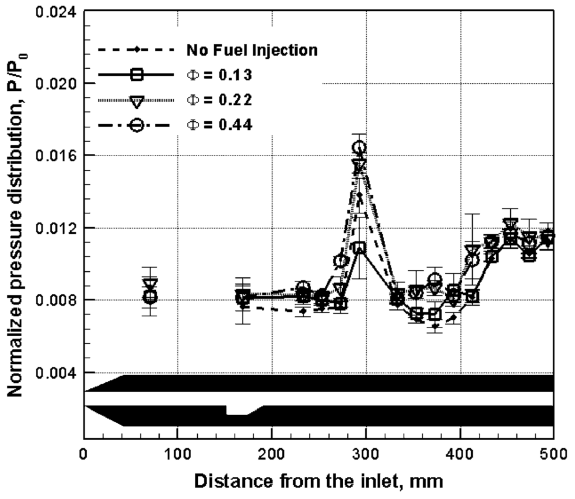

a)

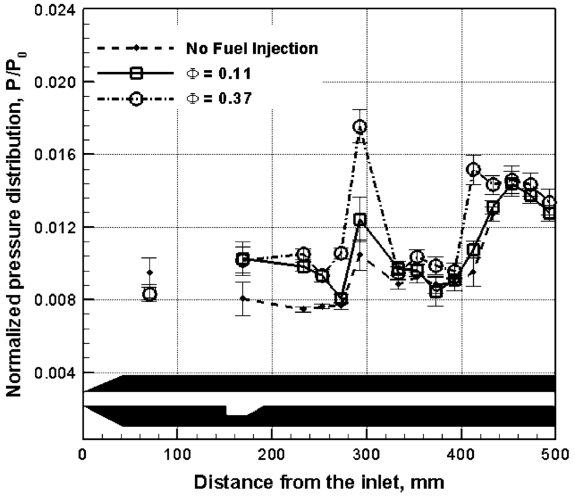

b)

Fig. 7 Wall pressure distribution of nonreacting flow. The total enthalpy of air is a) $h_0 = 6.45$ MJ/kg and b) $h_0 = 3.82$ MJ/kg.

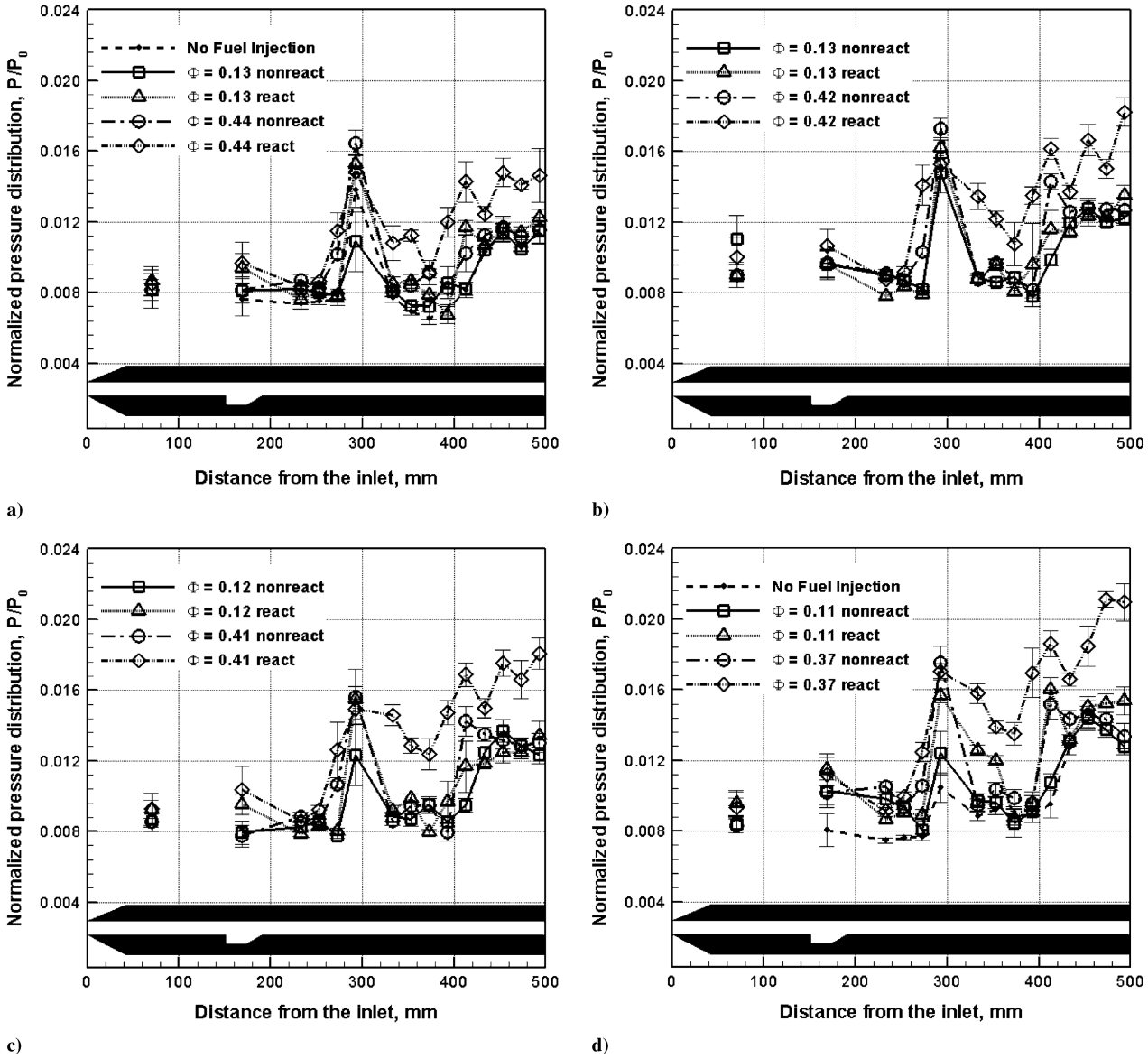

Fig. 8 Pressure comparison between nonreacting and reacting flow: a) $h_0 = 6.45$ MJ/kg, b) $h_0 = 5.16$ MJ/kg, c) $h_0 = 4.48$ MJ/kg, and d) $h_0 = 3.82$ MJ/kg.

lower at 6.45 MJ/kg and 15% lower at 3.82 MJ/kg than the combustor entrance static pressure, due to the influence of the expansion wave at the upstream corner of the cavity. Up to 100 mm downstream of the cavity, the pressures at the bottom wall are lower than the pressure at the combustor entrance because of the expansion wave formed at the cavity's trailing edge. As previously explained, the oblique shock on the cavity's rearward-facing step reflects from the top and bottom walls; consequently the highest pressure occurs approximately 290 mm from the duct entrance. When the total enthalpy is decreased from 6.45 to 3.82 MJ/kg, the static pressures measured 293 mm from the leading edge show different values for each enthalpy, given the possibility of the change of reflected shock position. Even though the absolute static pressure value is different at the reflected position, the overall pressure distribution in the combustor is similar for both conditions.

2. Nonreacting Flow

Figure 7 shows the static pressure distribution for nonreacting flow (injection of hydrogen into nitrogen) as the equivalence ratio and total enthalpy vary. Figures 7a and 7b are the results for total enthalpies of 6.45 and 3.82 MJ/kg, respectively. In Fig. 7a, the static pressures at $\Phi = 0.13$ are very similar to that of no fuel injection except at the first reflected shock position $x = 293$ mm. Therefore, the small fuel-mass flow rate does not have a significant effect on the static pressure in the combustor compared with no fuel injection. As the global equivalence ratio is increased by two (0.22) and 4 times (0.44), the static pressure distribution remains similar in form and rises in absolute terms by up to 25% in the downstream portion of the combustor. Even if fuel is injected with different injection pressure, the location of the overall static pressure fluctuation does not change significantly, although care needs to be exercised in interpreting peak pressures. The coarse spatial distribution of the transducers means that the actual peak floor static pressure may be up to 20 mm upstream or downstream of the peak measured pressure. In Fig. 7b, when hydrogen fuel is injected into low-total-enthalpy flow, the cavity's static pressure for the nonreacting flow is higher than that for no-fuel flow and does not vary with equivalence ratio. For low equivalence ratios, the static pressure values are similar to those for the no-fuel-injection case from the first reflected shock position near $x = 293$ mm. Likewise in Fig. 7a, the static pressure values rise when the fuel-mass flow is increased, showing that fuel addition alone may change the static pressures within the combustor by as much as 27%. This is described in more detail later in the paper. On the other hand, the pressure values are similar between low and high equivalence ratio conditions in the cavity and shock/expansion regions.

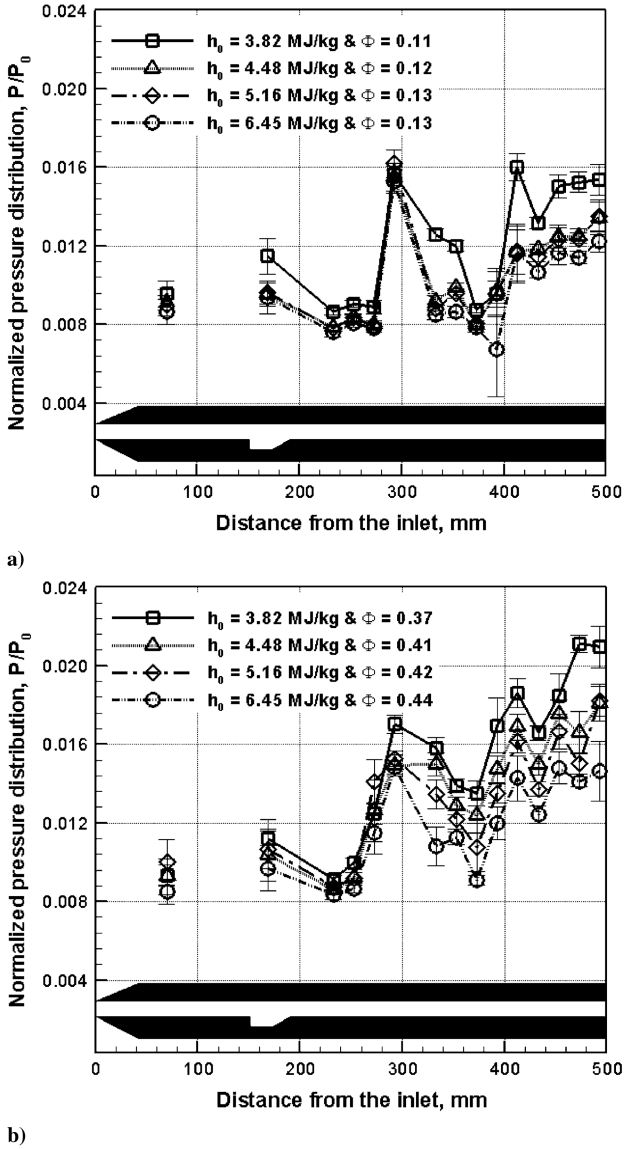

Fig. 9 Static pressure distribution for reacting flow: a) low Φ and b) high Φ.

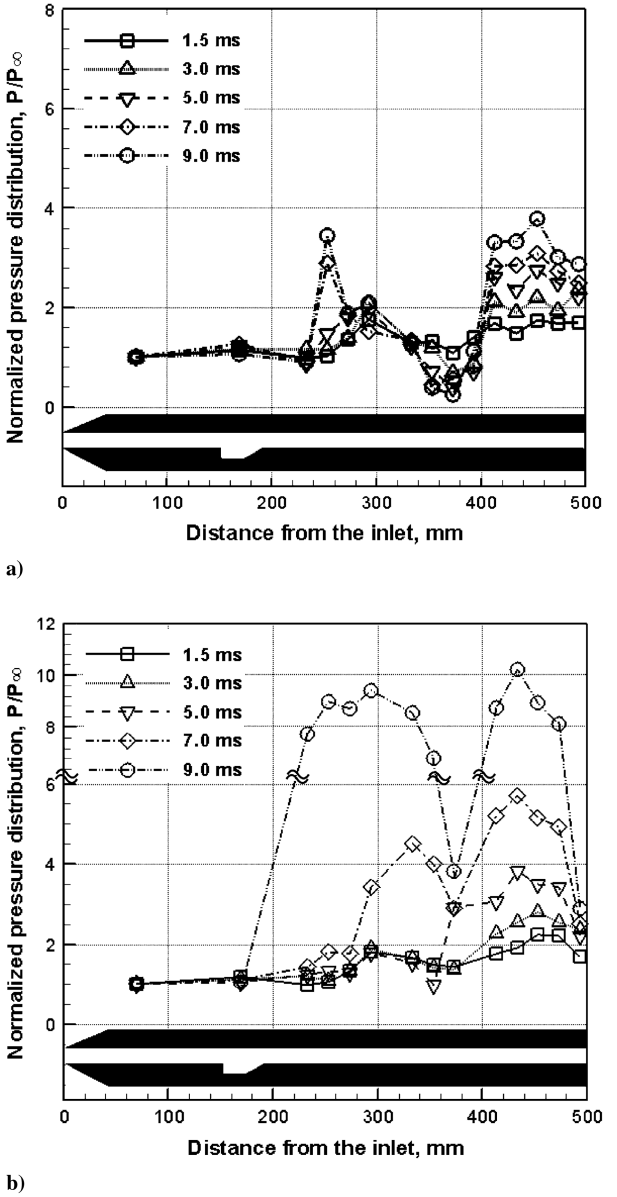

Fig. 10 Pressure traces for reacting flow according to time: a) $h_0 = 6.45$ MJ/kg and b) $h_0 = 3.82$ MJ/kg.

3. *Reacting Flow*

Figure 8 shows the static pressure comparisons for nonreacting and reacting flow at inlet total enthalpies of 6.45, 5.16, 4.48, and 3.82 MJ/kg. In Figs. 8a and 8c, the static pressure within the cavity is higher for reacting flow than for nonreacting flow, indicating that this pressure rise is due to the combustion generated near the cavity. But at a total enthalpy of 3.82 MJ/kg (Fig. 8d) there is a smaller static pressure difference in the cavity between reacting and nonreacting flow, with nearly the same static pressure values close to the cavity when the equivalence ratio is high. There may, therefore, be weak combustion near the cavity at low-total-enthalpy conditions, supporting the findings from the OH-PLIF images in Fig. 5. The fact that for the lower total enthalpy the relative increase in pressure due to combustion is lower in the cavity and higher downstream of the cavity can be explained by the fact that the ignition-delay time is longer at lower freestream temperatures. The highest static pressure appears near $x = 290$ mm in all cases (Figs. 8a–8d), so that even if the combustion occurred inside the cavity, the oblique shock generated at the rear cavity wall is reflected near this position for all air conditions. This indicates that the shock reflection near $x = 290$ mm generates most of the heat release in the flow. In Fig. 8, for all total enthalpy conditions the static pressure distributions between reacting and nonreacting flow are very similar to each other at the lower equivalence ratios. This means that even though combustion occurs at low equivalence ratios, it may be too weak to affect the pressure rise because of the weaker jet penetration into the main flow stream. There is evidence of a small increase in pressure downstream of the second shock-wave interaction with the jet, but the pressure soon decreases back to the same level as for injection into nitrogen, indicating that the combustion is most likely quenched by the expansion following the rear wall of the cavity. For all equivalence ratios, the static pressure values between the cavity's exit and 250 mm downstream of the inlet are similar to the noncombustion values. This region is influenced by the expansion wave generated by the cavity's trailing edge, so that the combustion is locally weak or extinguished in this region. For all total enthalpies, the static pressure values at a high equivalence ratio increase by more than 50% compared with those at a low equivalence ratio downstream of $x = 340$ mm. The relative increase is noticeably larger at lower total enthalpies. Especially in the case of reacting flow and a high equivalence ratio, a consistent offset of the static pressures along the duct compared with injection into nitrogen appears clearly in the downstream half of the combustor. Therefore supersonic combustion is generated in this model scramjet engine, with more consistent supersonic combustion at higher equivalence ratios.

Figure 9 shows the variation in combustor static pressure with total enthalpy at two equivalence ratios. At the low equivalence ratio (Fig. 9a), all static pressure distributions are very similar regardless of the total enthalpy, except at a total enthalpy of 3.82 MJ/kg. As described in Fig. 8, lower equivalence ratio overall leads to weak combustion in the duct. But as shown in Fig. 9b for the high equivalence ratio, as the total enthalpy is decreased the static pressures are increased. Also, the fluctuations of the static pressures in the duct show identical patterns so that the shock structures in the duct are similar regardless of the equivalence ratio. In Fig. 9b, the pressure values near the combustor exit (about $x = 470$ mm) at a total enthalpy of 3.82 MJ/kg increase more rapidly compared with the higher-enthalpy conditions.

Figure 10 shows the pressure distribution along the duct floor at different times during the tunnel run. Figures 10a and 10b indicate the results for $h_0 = 6.45$ and $h_0 = 3.82$ MJ/kg, respectively. If the instant when the incident shock reflects at the end of the shock tube is considered as $t = 0$, then the pressure values at 1.5, 3, 5, 7 and 9 ms are normalized by inlet pressure. The global equivalence ratio is $\Phi = 0.44$ for Fig. 10a and $\Phi = 0.37$ for Fig. 10b$t = 1.5$ ms. It must be noted that the shock-tunnel flow is characterized by reducing stagnation pressure, stagnation temperature, and total enthalpy as time passes, and so the equivalence ratio is increasing throughout the tunnel run. Also, the flow may contain some helium/argon driver gas from the compression tube at times greater than approximately 4 ms after shock reflection. For Fig. 10a, even though the pressure values are different, the pressure fluctuations are sustained in the duct as time passes, with the pressure traces indicating supersonic flow throughout the test time. But Fig. 10b shows a different configuration compared with Fig. 10a, and it has a sudden pressure increase at positions of 450, 370, 350, and 260 mm downstream of the combustor entrance and close to the cavity when the time is 1.5, 3, 5, 7, and 9 ms after shock reflection at the nozzle reservoir, respectively. These phenomena indicate thermally choked flow. Regardless of whether flow is subsonic or supersonic, chemical-heat-release results in the local Mach number tend toward unity. In this experiment, the heat release in the supersonic flow produces a thermally-induced compression wave. When the heat is released too rapidly, the flow is thermally choked and generates a sonic line. If more heat is supplied continuously, this compression wave is changed into a strong normal shock, and the combustor experiences thermal blockage, with the shock wave moving rapidly upstream. According to the measured pressure distribution, the condition at $h_0 = 3.82$ MJ/kg and $\Phi = 0.37$ has thermal choking in the duct from $t = 5$ ms. For the test condition of $h_0 = 3.82$ MJ/kg, the inflow density is higher than at the higher total enthalpies, and so this condition more readily induces thermal choking. Even though this paper does not include any schlieren images of thermally-choked flow, the graphs in Fig. 10 show temporary thermal choking in the downstream part of the combustor, thermal blockage, and rapid movement upstream of a pressure disturbance caused by additional heat release. Similar behavior has been noted by O'Byrne et al. in previous combustor experiments performed in the same facility using a strut injector configuration [37].

Figure 11 shows the combustion effect when the pressures for reacting and nonreacting flow are each divided by their stagnation pressure, and then the reacting pressure ratio is divided by the nonreacting pressure ratio at the same location. Dividing each trace by the reservoir pressure reduces fluctuations caused by run-to-run variations in reservoir pressure, and dividing the two ratios allows the effect of combustion to be seen clearly. Independent of the equivalence ratio, the 3.82 MJ/kg condition has little combustion effect up to $x = 240$ mm, and the lack of a pressure rise indicates little or no combustion near the cavity. The 3.82 MJ/kg condition has a combustor inlet temperature of 900 K, and, therefore, has a relatively long ignition-delay time. Davis and Bowersox [23,24] proposed a relationship between cavity-residence time τ_r, cavity depth D, and freestream velocity U_∞, given by $\tau_r = 40 \cdot U_\infty / D$. Using this equation, the cavity-residence time is 6.77×10^{-5} s at $h_0 = 6.45$ MJ/kg and 8.52×10^{-5} s at $h_0 = 3.82$ MJ/kg, indicating very similar residence times across the range of conditions

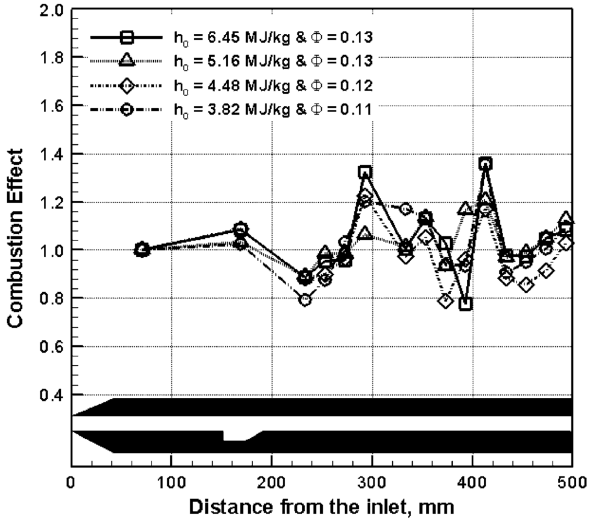

a)

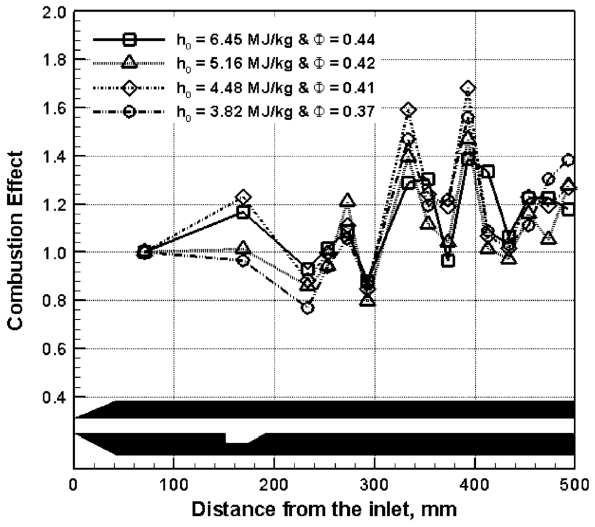

b)

Fig. 11 Combustion effect for varying total-enthalpy conditions: a) low Φ and b) high Φ.

investigated here. Colket and Spadaccini [38] proposed the effects of initial oxygen concentration (pressure) and temperature on the ignition-delay times of hydrogen–oxygen mixtures. In this research, the oxygen mole fraction at the inlet is 0.172 at $h_0 = 6.45$ MJ/kg and 0.185 of $h_0 = 3.82$ MJ/kg. From Colket and Spadaccini's relations, the ignition-delay times are 4.58×10^{-6} and 4.32×10^{-4} s at $h_0 = 6.45$ and $h_0 = 3.82$ MJ/kg, respectively. Therefore, cavity-residence time can be longer than ignition-delay time for $h_0 = 6.45$ MJ/kg and allow more time for the cavity to act as a flame holder. Flow for the $h_0 = 3.82$ MJ/kg condition, however, needs 100 times the ignition-delay time of the $h_0 = 6.45$ MJ/kg condition, making flame holding in the cavity less likely. These results support the explanations of the measured OH fluorescence signal distribution of Fig. 5 and the cavity's pressure measurements of Fig. 8. Also, the expansion wave downstream of the cavity's leading edge will decrease the flow temperature and act to inhibit flame formation. But after the shock reflection in the middle region of the duct, combustion occurs more actively compared with the first half of the combustor. This shock reflection increases the fuel–air mixing and generates combustion as an ignitor by spontaneous pressure rise. The pressure distributions at a low equivalence ratio shown in Fig. 11a are formed by the reflected shock structure and show the extinguishing of heat release by expansions at some locations in the duct. However, a high equivalence ratio flows in Fig. 11b induce the whole flame behind the middle of the combustor and shock structures control the flame

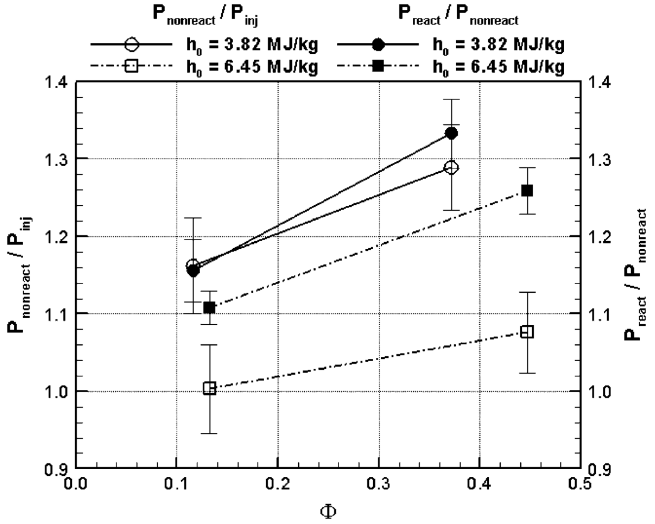

Fig. 12 Averaged pressures behind the 400 mm of the combustor.

shape, as shown by the alternating high- and low-pressure ratios in the plot. The less-than-unity pressure ratios in the upstream portions of the plots in Fig. 11 are caused by differences in the locations of the shock waves between injection into air and injection into nitrogen.

Figure 12 shows the averaged ratios of nonreacting to noninjection pressure and reacting to nonreacting pressure for the five pressure transducers located more than 400 mm downstream of the combustor entrance. Regardless of the total enthalpy, the averaged pressure ratios of nonreacting to noninjection pressure increase as the equivalence ratio increases. This shows that, as described previously, the mass addition of fuel increases the pressure in the combustor. The averaged pressure ratios of reacting to nonreacting pressure show the overall effect of varying enthalpy and equivalence ratio on the flow at the exit of the combustor. For all stagnation enthalpies there is a trend of increasing pressure rise due to combustion with an increasing equivalence ratio, most likely caused by increased penetration of the fuel jet into the combustor airflow. The average pressure ratio at total enthalpy $h_0 = 3.82$ MJ/kg is higher than at other inflow conditions due to additional combustion heat release to the flow and shows an average pressure increase rate as high as 33% at the higher equivalence ratio.

Comparison of the results in Figs. 5 and 12 show opposing trends. The OH-PLIF images in Fig. 5 indicate that higher stagnation enthalpies lead to better ignition near the cavity, whereas the pressure rise due to combustion in Fig. 12 indicates an overall higher pressure rise due to combustion at the lower stagnation enthalpy condition. It appears that the combustion behavior in this flow is dominated by ignition from the reflected shocks from the cavity's trailing face rather than the effect of storage of OH within the cavity itself.

IV. Conclusions

This study describes the mixing and ignition processes in a model scramjet combustor using OH planar laser-induced fluorescence visualization and time-resolved floor static pressure measurements. Experiments at several airflow total enthalpies and global fuel–air equivalence ratios indicate the following:

1) The separated shear layer in the main flow reattaches and generates an oblique shock wave at the cavity's trailing edge. Over the range of freestream total-enthalpy conditions used in this study, the flow structures caused by the oblique shock are similar.

2) The oblique shock structures for nonreacting flow still build in the same manner as for the case of no fuel injection, and the fuel layer interacts with the trailing-edge shock, actively mixing with the airstream. A low-equivalence ratio has a small effect on static pressure, but as the equivalence ratio is increased the static pressures rise due to combustion. However, the overall shape of the pressure distribution throughout the combustor does not change in spite of the different fuel-injection pressure for angled injection. Therefore, the cavity geometry has the greatest effect on the shape of the pressure distribution in this study.

3) Some evidence of the cavity acting as a flame holder can be seen from Fig. 5, as some OH can be seen within the cavity. This is different behavior than that noted in a previous study in which fuel is injected from the rear step of the cavity and OH formation occurred only in the shear layer above the cavity. However, the concentrations in the cavity are low, and most of the combustion still appears to be occurring in the shear layer above the cavity. A low equivalence ratio does not ignite at the injection location due to the fuel jet being too close to the cold wall and not producing a strong enough bow shock, but at the higher equivalence ratios the flow starts to ignite immediately upstream of the injector, because of flow separation caused by the bow shock in front of the jet. High fuel-injection pressure forms two flame layers in the two-dimensional OH signal image. Periodic OH peak signal appears to be caused by oscillating cavity flow or oscillation of the fuel jet, and the interval between OH peak signals becomes shorter as the equivalence ratio increases. At lower total enthalpy conditions, the static pressure distribution in the cavity is similar to that of nonreacting flow due to weak combustion. For the higher equivalence ratios, the static pressures increase by up to 50% over the noncombustion case, and this effect becomes more significant as the total enthalpy is decreased. The combination of low total enthalpy and a high equivalence ratio leads to thermal choking, beginning at the downstream part of the combustor because of the greater heat release at lower enthalpy conditions, and the reduction in pressure and total enthalpy of the freestream at the later times. Ignition-delay length increases as total enthalpy decreases, due to the reduced reaction rates at lower freestream temperatures.

Finally, comparing the visualizations of the cavity flow and the static pressure rise in the downstream portion of the combustor indicates that although the cavity may contain OH, most of the upstream OH is generated in the shear layer above the cavity, and the cavity's effect on the overall heat release is secondary to the effect of the oblique shock wave generated by the rear face of the cavity at these flow conditions.

Acknowledgments

This work is a collaboration between research groups at Australian National University, University of New South Wales, Australian Defence Force Academy, and Seoul National University, supported by the second stage of the Brain Korea 21 and the National Research Laboratory program of the Korea Science and Engineering Foundation (KOSEF) (M10500000072-05J000007210). The authors wish to acknowledge this financial support. The authors also thank Paul Walsh for his technical assistance in performing the experiments.

References

[1] Ferri, A., "Mixing-Controlled Supersonic Combustion," *Annual Review of Fluid Mechanics*, Vol. 5, No. 1, 1973, pp. 301–338. doi:10.1146/annurev.fl.05.010173.001505

[2] Kumar, A., Bushnell, D. M., and Hussaini, M. Y., "Mixing Augmentation Technique for Hypervelocity Scramjets," *Journal of Propulsion and Power*, Vol. 5, No. 5, 1989, pp. 514–522. doi:10.2514/3.23184

[3] Lee, S.-H., and Mitani, T., "Mixing Augmentation of Transverse Injection in Scramjet Combustor," *Journal of Propulsion and Power*, Vol. 19, No. 1, 2003, pp. 115–124.

[4] Tomioka, S., Jacobsen, L. S., and Schetz, J. A., "Sonic Injection from Diamond-Shaped Orifices into a Supersonic Crossflow," *Journal of Propulsion and Power*, Vol. 19, No. 1, 2003, pp. 104–114.

[5] Everett, D. E., Woodmansee, M. A., Dutton, J. C., and Morris, M. J., "Wall Pressure Measurements for a Sonic Jet Injected Transversely into a Supersonic Crossflow," *Journal of Propulsion and Power*, Vol. 14, No. 6, 1998, pp. 861–868.

[6] Sunami, T., Magre, P., Bresson, A., Grisch, F., Orain, M., and Kodera, M., "Experimental Study of Strut Injectors in a Supersonic Combustor Using OH-PLIF," AIAA Paper 2005-3304, May 2005.

[7] Riggins, D. W., and Vitt, P. H., "Vortex Generation and Mixing in Three-Dimensional Supersonic Combustors," *Journal of Propulsion and Power*, Vol. 11, No. 3, 1995, pp. 419–426. doi:10.2514/3.23860

[8] Jacobsen, L. S., Gallimore, S. D., Schetz, J. A., O'Brien, W. F., and Goss, L. P., "Improved Aerodynamic-Ramp Injector in Supersonic Flow," *Journal of Propulsion and Power*, Vol. 19, No. 4, 2003, pp. 663–673.

[9] Sung, C. J., Li, J. G., Yu, G., and Law, C. K., "Chemical Kinetics and Self-Ignition in a Model Supersonic Hydrogen-Air Combustor," *AIAA Journal*, Vol. 37, No. 2, 1999, pp. 208–214.

[10] Owens, M. G., Mullagiri, S., Segal, C., Ortwerth, P. J., and Mathur, A. B., "Thermal Choking Analyses in a Supersonic Combustor," *Journal of Propulsion and Power*, Vol. 17, No. 3, 2001, pp. 611–616.

[11] Huber, P. W., Schexnayder, C. J., Jr., and McClinton, C. R., "Criteria for Self-Ignition of Supersonic Hydrogen-Air Mixtures," NASA TP-1457, 1979.

[12] Ben-Yakar, A., and Hanson, R. K., "Experimental Investigation of Flame-Holding Capability of Hydrogen Transverse Jet in Supersonic Cross-Flow," *Proceeding of the Twenty-Seventh International Symposium on Combustion*, The Combustion Institute, Pittsburgh, PA, 1998, pp. 2173–2180.

[13] Seiner, J. M., Dash, S. M., and Kenzakowski, D. C., "Historical Survey on Enhanced Mixing in Scramjet Engines," *Journal of Propulsion and Power*, Vol. 17, No. 6, 2001, pp. 1273–1286.

[14] Lee, S.-H., "Characteristics of Dual Transverse Injection in Scramjet Combustor, Part 1: Mixing," *Journal of Propulsion and Power*, Vol. 22, No. 5, 2006, pp. 1012–1019.
doi:10.2514/1.14180

[15] Kuratani, N., Ikeda, Y., Nakajima, T., Tomioka, S., and Mitani, T., "Mixing Characteristics of Normal Injection into a Supersonic Backward-Facing Step Flow Measured with PIV," AIAA Paper 2002-237, Jan. 2002.

[16] Abbitt, J. D., Segal, C., McDaniel, J. C., Krauss, A. H., and Whitehurst, R. B., "Experimental Supersonic Hydrogen Combustion Employing Staged Injection Behind a Rearward-Facing Step," *Journal of Propulsion and Power*, Vol. 9, No. 3, 1993, pp. 472–478.
doi:10.2514/3.23646

[17] Riggins, D. W., McClinton, C. R., Rogers, R. C., and Bittner, R. D., "Investigation of Scramjet Injection Strategies for High Mach Number Flows," *Journal of Propulsion and Power*, Vol. 11, No. 3, 1995, pp. 409–418.
doi:10.2514/3.23859

[18] McMillin, B. K., Seitzman, J. M., and Hanson, R. K., "Comparison of NO and OH Planar Fluorescence Temperature Measurements in Scramjet Model Flowfields," *AIAA Journal*, Vol. 32, No. 10, 1994, pp. 1945–1952.
doi:10.2514/3.12237

[19] Schneider, F., Gerlinger, P., and Aigner, M., "Enhanced Mixing in Supersonic Combustion," *High Performance Computing in Science and Engineering '04*, Springer–Verlag, Heidelberg, Germany, 2005.

[20] Ben-Yakar, A., and Hanson, R. K., "Cavity Flame-Holders for Ignition and Flame Stabilization in Scramjets: An Overview," *Journal of Propulsion and Power*, Vol. 17, No. 4, 2001, pp. 869–877.

[21] Vinogradov, V. A., Kobigski, S. A., and Petrov, M. D., "Experimental Investigation of Kerosene Fuel Combustion in Supersonic Flow," *Journal of Propulsion and Power*, Vol. 11, No. 1, 1995, pp. 130–134.
doi:10.2514/3.23850

[22] Ortweth, P., Mathur, A., Vinogradov, V., Grin, V., Goldfeld, M., and Starov, A., "Experimental and Numerical Investigation of Hydrogen and Ethylene Combustion in a Mach 3–5 Channel with a Single Injector," AIAA Paper 1996-3245, July 1996.

[23] Davis, D. L., and Bowersox, R. D. W., "Stirred Reactor Analysis of Cavity Flame Holders for Scramjets," AIAA Paper 1997-3274, July 1997.

[24] Davis, D. L., and Bowersox, R. D. W., "Computational Fluid Dynamics Analysis of Cavity Flame Holders for Scramjets," AIAA Paper 1997-3270, July 1997.

[25] Gruber, M. R., Baurle, R. A., Mathur, T., and Hsu, K.-Y., "Fundamental Studies of Cavity-Based Flameholder Concepts for Supersonic Combustors," *Journal of Propulsion and Power*, Vol. 17, No. 1, 2001, pp. 146–153.

[26] Donbar, J. M., Gruber, M. R., Jackson, T. A., Carter, C. D., and Mathur, T., "OH Planar Laser-Induced Fluorescence Imaging in a Hydrocarbon-Fueled Scramjet Combustor," *Proceeding of the Twenty-Eighth International Symposium on Combustion*, The Combustion Institute, Pittsburgh, PA, 2000, pp. 679–687.

[27] Gruber, M. R., Donbar, J. M., Carter, C. D., and Hsu, K.-Y., "Mixing and Combustion Studies Using Cavity-Based Flameholders in a Supersonic Flow," *Journal of Propulsion and Power*, Vol. 20, No. 5, 2004, pp. 769–778.
doi:10.2514/1.5360

[28] O'Byrne, S., Stotz, I., Neely, A. J., Boyce, R. R., Mudford, N. R., and Houwing, A. F. P., "OH PLIF Imaging of Supersonic Combustion Using Cavity Injection," AIAA Paper 2005-3357, May 2005.

[29] Neely, A. J., Stotz, I., O'Byrne, S., Boyce, R. R., Mudford, N. R., and Houwing, A. F. P., "Flow Studies on a Hydrogen-Fueled Cavity Flame-Holder Scramjet," AIAA Paper 2005-3358, May 2005.

[30] Stalker, R. J., "Development of a Hypervelocity Wind Tunnel," *The Aeronautical Journal*, Vol. 76, No. 738, 1972, pp. 374–384.

[31] O'Byrne, S., "Examination of Transient Mixing and Combustion Processes in a Supersonic Combustion Ramjet Engine," Master's Thesis, Dept. of Physics, Australian National Univ., 1997.

[32] McIntosh, M. K., "Computer Program for the Numerical Calculation of Frozen Equilibrium Conditions in Shock Tunnels," Australian National Univ., Canberra, Australia, 1968.

[33] Vardavas, I. M., "Modelling Reactive Gas Flows Within Shock Tunnels," *Australian Journal of Physics*, Vol. 37, No. 2, 1984, pp. 157–177.

[34] Seitzman, J. M., and Hanson, R. K., "Comparison of Excitation Techniques for Quantitative Fluorescence Imaging of Reacting Flows," *AIAA Journal*, Vol. 31, No. 3, 1993, pp. 513–519.
doi:10.2514/3.11359

[35] Ben-Yakar, A., and Hanson, R. K., "Supersonic Combustion of Cross-Flow Jets and the Influence of Cavity Flame-Holders," AIAA Paper 1999-484, Jan. 1999.

[36] Vakili, A. D., and Gauthier, C., "Control of Cavity Flow by Upstream Mass-Injection," *Journal of Aircraft*, Vol. 31, No. 1, 1994, pp. 169–174.
doi:10.2514/3.46470

[37] O'Byrne, S., Doolan, M., Olsen, S. R., and Houwing, A. F. P., "Analysis of Transient Thermal Choking Processes in a Model Scramjet Engine," *Journal of Propulsion and Power*, Vol. 16, No. 5, 2000, pp. 808–814.

[38] Colket, M. B., III, and Spadaccini, L. J., "Scramjet Fuels Autoignition Study," *Journal of Propulsion and Power*, Vol. 17, No. 2, 2001, pp. 315–323.

R. Bowersox
Associate Editor